Inorg. Chem. **2006**, *45*, 7628–7641

Evolution of the Structural Chemistry of Vanadium Organodiphosphonate Networks and Frameworks: Structural Consequences of Fluoride Incorporation in the Development of Stable Phases with Void Channels

Wayne Ouellette,[†] Ming Hui Yu,[‡] Charles J. O'Connor,[‡] and Jon Zubieta*[,†]

Department of Chemistry, Syracuse University, Syracuse, New York 13244-4100 and Advanced Materials Research Institute, University of New Orleans, New Orleans, Louisiana 70148

Received March 15, 2006

Hydrothermal reactions of solutions containing a vanadate source, an organodiphosphonate, an organonitrogen component, and HF (V/P/O/F) yield a series of oxyfluorovanadium–diphosphonates with charge-compensation provided by organoammonium cations or hydronium cations. While V/P/O/F networks provide the recurrent structural motif, the linkage between the layers and the details of the polyhedral connectivities within the layers are quite distinct for the five structures of this study. $[H_2pip][V_4F_4O_2(H_2O)_2\{O_3P(CH_2)_3PO_3\}_2]$ (**1**) (pip = piperazine) is a conventional three-dimensional (3D) "pillared" layer structure, whose V/P/O/F networks are buttressed by the propylene chains of the diphosphonate ligands. In contrast, $[H_2en][V_2O_2F_2(H_2O)_2\{O_3P(CH_2)_4PO_3\}]$ (**2**) and $[H_2en]_2[V_6F_{12}(H_2O)_2\{O_3P(CH_2)_5PO_3\}_2\ \{HO_3P(CH_2)_5PO_3H\}]$ (**3**) are two-dimensional (2D) slablike structures constructed of pairs of V/P/O/F networks sandwiching the pillaring organic tethers of the diphosphonate ligands. Despite the common overall topology, the layer substructures are quite different: isolated $\{VO_5F\}$ octahedra in **2** and chains of corner-sharing $\{VO_3F_3\}$ octahedra in **3**. The 3D structure of $[H_2en]_2[V_7O_6F_4(H_2O)_2\{O_3P(CH_2)_2PO_3\}_4]\cdot 7H_2O$ (**4**·$7H_2O$) exhibits a layer substructure that contains the ethylene bridges of the diphosphonate ligands and are linked through corner-sharing octahedral $\{VO_6\}$ sites. The connectivity requirements provide large channels that enclose readily removed water of crystallization. The structure of $[H_3O][V_3F_2(H_2O)_2\{O_3P(CH_2)_2PO_3\}_2]\cdot 3.5H_2O$ (**5**·$3.5H_2O$) is also 3D. Because of the similiarity with **4**·$7H_2O$, it exhibits V/P/O/F layers that include the organic tethers of the diphosphonates and are linked through corner-sharing $\{VO_6\}$ octahedra. In contrast to the network substructure of **4**·$7H_2O$, which contains binuclear and trinuclear vanadium clusters, the layers of **5**·$3.5\ H_2O$ are constructed from chains of corner-sharing $\{VO_4F_2\}$ octahedra. Thermal studies of the open framework materials 4 and 5 reveal that incorporation of fluoride into the inorganic substructures provides robust scaffoldings that retain their crystallinity to 450 °C and above. In the case of **4**, dehydration does not change the powder X-ray diffraction pattern of the material, which remains substantially unchanged to 450 °C. In the case of **5**, there are two dehydration steps, that is, the higher temperature process associated with loss of coordinated water. This second dehydration results in structural changes as monitored by powder X-ray diffraction, but this new phase is retained to ca. 450 °C. The materials of this study exhibit a range of reduced oxidation states: **1** is mixed valence V(IV)/V(III) while **2** and **4**·$7H_2O$ are exclusively V(IV) and **3** and **5**·$3.5H_2O$ are exclusively V(III). These oxidation states are reflected in the magnetic properties of the materials. The paramagnetism of **1** arises from the presence of V(III) and V(IV) sites and conforms to the Curie–Weiss law with $C = 2.38$ em K/(Oe mol) and $\Theta = -66$ K with μ_{eff} (300 K) = 4.33 μ_B. Compounds **3**–**5** exhibit Curie–Weiss law dependence of magnetism on temperature with μ_{eff} (300 K) = 5.45 μ_B for **3** (six V(III) sites), $\mu_{eff} = 4.60\ \mu_B$ for **4** (seven V(IV) sites) and $\mu_{eff} = 4.13\ \mu_B$ for **5** (two V(III) sites). Compound **2** exhibits antiferromagnetic interactions, and the magnetism may be described in terms of the Heisenberg linear antiferromagnetic chain model for V(IV). The effective magnetic moment at 300 K is 2.77 μ_B (two V(IV) sites).

Introduction

Hybrid organic−inorganic materials occupy a prominent position among the new classes of materials enjoying widespread contemporary interest by virtue of their applications to catalysis,[1−3] optical materials,[4−6] membranes,[7] and sorption.[8−13] The diversity of properties associated with these materials reflects a vast compositional range, which allows variations in covalency, geometry, and oxidation states, as

* To whom correspondence should be addressed. E-mail: jazubiet@syr.edu. Telfax: International code + (315)-443-4070.
[†] Syracuse University.
[‡] University of New Orleans.

(1) Ngo, H. L.; Hu, A. G.; Lin, W. B. *J. Mol. Catal. A* **2004**, *215*, 177.
(2) Forster, P. M.; Cheetham, A. K. *Top. Catal.* **2003**, *24*, 1.

10.1021/ic0604462 CCC: $33.50
Published on Web 08/23/2006

well as a versatile crystalline architecture,[14] which may provide different pore structures, coordination sites, or juxtapositions of functional groups.[15−18]

On the basis of a molecular scale composite of inorganic and organic components, these complex structures provide the potential for the design of novel functional materials.[19] The inorganic component may provide electrical mobility, unusual magnetic, dielectric, or optical properties, mechanical hardness, and thermal stability. Similarly, organic molecules offer processability, structural diversity, a range of polarizabilities, and useful luminescence properties. Consequently, the combination of the unique features of organic and inorganic compounds in a complementary fashion in the hybrid materials may lead to unusual solid-state structures and materials with composite or novel properties that provide access to a vast area of complex, multifunctional materials.

In organic−inorganic hybrid materials, both the inorganic and organic components are integral parts of an extended structure. The design of organic−inorganic hybrid materials conceives of the metal, metal cluster, or metal oxide substructure as a node from which rigid or flexible multitopic organic ligands radiate to act as tethers to adjacent nodes in the bottom-up construction of complex extended architectures. Two categories of such materials have been identified: metal organic frameworks (MOFs) or coordination polymers in which metal atoms or clusters are bridged by polyfunctional organic molecules, and metal oxide hybrids in which metal−oxygen−metal (M−O−M or M−O−M′) arrays are embedded within the architectures.

The vanadium−organophosphonates[20] represent a prototypical family of organic−inorganic hybrid materials that exhibit considerable structural diversity and useful sorptive properties.[21−44] We demonstrated in a recent contribution[21] that these materials possess structurally well-defined internal void spaces whose dimensions and juxtaposition relative to the inorganic oxide scaffold may be influenced by the choice of charge-balancing cations and/or the identity of the organophosphonate component.

The syntheses of the materials of the oxovanadium−organodiphosphonate class previously described by us exploited HF to effect mineralization and to induce crystallization at the acidic pH of the reactions. It was noted that increasing the amount of HF introduced in the synthesis allowed the incorporation of fluoride into the inorganic oxide substructures to produce oxyfluorinated materials.

The structural consequences of fluoride incorporation were investigated for the three component system $\{Cu_2(\text{bisterpy})\}^{4+}/V_xO_yF_z^{n-}/\{O_3P(CH_2)_nPO_3\}^{4-}$ (bisterpy = 2,2′:4′,4″:2″:2‴-quaterpyridyl-6,6″-di-2-pyridine)[45] in which the two oxide components react to provide the anionic oxyfluorovanadate−diphosphonate framework, while the complex coordination cation provides charge compensation. In contrast to the structurally less diverse nonfluorinated materials of the type $\{Cu_2(\text{bisterpy})\}^{4+}/V_xO_y^{n-}/\{O_3P(CH_2)_nPO_3\}$,$^{4-}$ the fluorinated phases exhibit a range of V/P/O/F (hydrothermal reactions of solutions containing a vanadate source, an organodiphosphonate, an organonitrogen component, and HF) building blocks such as embedded clusters, chains and networks, and

(3) Janiak, C. *Dalton Trans.* **2003**, 2781.
(4) Sanchez, C.; Lebeau, B.; Chaput, F.; Boilot, J. P. *Adv. Mater. (Weinham, Ger.)* **2003**, *15*, 1969.
(5) Evans, O. R.; Lin, W. B. *Chem. Mater.* **2001**, *13*, 3009.
(6) Evans, O. R.; Lin, W. B. *Acc. Chem. Res.* **2002**, *35*, 511.
(7) Javaid, P. *Curr. Opin. Colloid Interface Sci.* **2003**, *8*, 96.
(8) Sudik, A. C.; Millward, A. R.; Ockwig, N. W.; Coté, A. P.; Kim, J.; Yaghi, O. M. *J. Am. Chem. Soc.* **2005**, *127*, 2110.
(9) Kesanli, B.; Lin, W. B. *Coord. Chem. Rev.* **2003**, *246*, 305.
(10) Cingolani, A.; Galli, S.; Masciocchi, N.; Pandolfo, L.; Pettinari, C.; Sironi, A. *J. Am. Chem. Soc.* **2005**, *127*, 6144.
(11) Wu, C. D.; Lin, W. *Angew. Chem., Int. Ed.* **2005**, *44*, 1958.
(12) Ahmori, O.; Kawano, M.; Fujita, M. *Angew. Chem., Int. Ed.* **2005**, *44*, 1962, and references therein.
(13) Lee, E. Y.; Jany, S. Y.; Suh, M. P. *J. Am. Chem. Soc.* **2005**, *127*, 6374.
(14) James, S. L. *Chem. Soc. Rev.* **2003**, *32*, 276.
(15) Kaskel, S.; Porous Metal-Organic Frameworks. In *Handbook of Porous Solids*; Schüth F., Sing, K. S. W., Weitkamp, J., Eds.; Wiley-VCH: Weinham, Germany, 2002; Vol. 2, p 1190.
(16) Bu, X.; Feng, P. *Chem. Nanostruct. Mater.* **2003**, 1.
(17) Roesseinsky, M. J. *Microporous Mesoporous Mater.* **2004**, *73*, 15.
(18) Rosi, N. L.; Kim, J.; Eddaoudi, M.; Chen, B.; O'Keeffe, M.; Yaghi, O. M. *J. Am. Chem. Soc.* **2005**, *127*, 1504.
(19) Mitzi, D. M. *Dalton Trans.* **2001**, 1.
(20) The chemistry of metal organophosphonates has been the subject of extensive study since the pioneering work of Clearfield and Alberti. (a) Clearfield, A. *Curr. Opin. Solid State Mater. Sci.* **2003**, *6*, 495. (b) Clearfield, A. *Prog. Inorg. Chem.* **1998**, *47*, 371. (c) Alberti, G. In *Comprehensive Supramolecular Chemistry*; Atwood, J. L., Davis, J. E. D., Vogel, F., Eds.; Pergamon Press: New York, 1996; Vol. 9, p 182.
(21) Ouellette, W.; Koo, B.-K.; Burkholder, E.; Golub, V.; O'Connor, C. J.; Zubieta, J. *Dalton Trans.* **2004**, 1527.
(22) Finn, R. C.; Zubieta, J.; Haushalter, R. C. *Prog. Inorg. Chem.* **2003**, *51*, 451.
(23) Riou-Cavellec, M.; Sanselme, M.; Férey, G. *J. Mater. Chem.* **2000**, *10*, 745.
(24) Huan, G.; Johnson, J. W.; Jacobson, A. J.; Merola, J. S. *J. Solid State Chem.* **1990**, *89*, 220.
(25) Harrison, W. T. A.; Dussack, L. L.; Jacobson, A. J. *Inorg. Chem.* **1996**, *35*, 1461.
(26) Khan, M. I.; Zubieta, J. *Prog. Inorg. Chem.* **1995**, *43*, 1.
(27) Khan, M. I.; Lee, Y.-S.; O'Connor, C. J.; Haushalter, R. S.; Zubieta, J. *Inorg. Chem.* **1994**, *33*, 3855.
(28) Khan, M. I.; Lee, Y.-S.; O'Connor, C. J.; Haushalter, R. S.; Zubieta, J. *Chem. Mater.* **1994**, *6*, 4525.
(29) Khan, M. I.; Lee, Y.-S.; O'Connor, C. J.; Haushalter, R. S.; Zubieta, J. *Chem. Mater.* **1994**, *6*, 721.
(30) Soghomonian, V.; Chen, Q.; Haushalter, R. C.; Zubieta, J. *Angew. Chem., Int. Ed.* **1995**, *34*, 4460.
(31) Soghomonian, V.; Diaz, R.; Haushalter, R. C.; O'Connor, C. J.; Zubieta, J. *Inorg. Chem.* **1995**, *34*, 4460.
(32) Soghomonian, V.; Haushalter, R. C.; Zubieta, J. *Chem. Mater.* **1995**, *7*, 1648.
(33) Bonavia, G.; Haushalter, R. C.; O'Connor, C. J.; Zubieta, J. *Inorg. Chem.* **1996**, *35*, 5603.
(34) Ninclaus, C.; Serre, C.; Riou, D.; Férey, G. *C. R. Acad. Sci., Ser. IIc: Chim.* **1998**, *1*, 551.
(35) Bonavia, G.; Haushalter, R. C.; Lu, S.; O'Connor, C. J.; Zubieta, J. *J. Solid State Chem.* **1997**, *132*, 144.
(36) Riou, D.; Serre, C.; Férey, G. *J. Solid State Chem.* **1998**, *141*, 89.
(37) Riou, D.; Roubeau, O.; Férey, G. *Microporous Mesoporous Mater.* **1998**, *23*, 23.
(38) Riou, D.; Férey, G. *J. Mater. Chem.* **1998**, *8*, 2733.
(39) Yucesan, G.; Golub, V.; O'Connor, C. J.; Zubieta, J. *Dalton Trans.* **2005**, 2241.
(40) Yucesan, G.; Golub, V.; O'Connor, C. J.; Zubieta, J. *Solid State Sci.* **2005**, *7*, 133.
(41) Yucesan, G.; Ouellette, W.; Golub, V.; O'Connor, C. J.; Zubieta, J. *Solid State Sci.* **2005**, *7*, 445.
(42) Yucesan, G.; Yu, M. H.; Ouellette, W.; O'Connor, C. J.; Zubieta, J. *Cryst Eng Comm* **2005**, *7*, 480.
(43) Yucesan, G.; Yu, M.-H.; O'Connor, C. J.; Zubieta, J. *Cryst Eng Comm* **2005**, *7*, 711.
(44) Ouellette, W.; Yu, M. H.; O'Connor, C. J.; Zubieta, J. *Inorg. Chem.* **2006**, *8*, 3224-3239.
(45) Ouellette, W.; Golub, V.; O'Connor, C. J.; Zubieta, J. *Dalton Trans.* **2005**, 291.

even three dimensional (3D) frameworks. Furthermore, while the $\{Cu_2(bisterpy)\}^{4+}/V_xO_y^{n-}$/diphosphonate family of materials revealed no instances of directly linked vanadium polyhedra in the oxide substructures, the fluorinated species exhibited several structures with V−O−V (vanadium−oxygen−vanadium) bonds in entrained binuclear and/or tetranuclear oxovanadium subunits. In addition to the expansive structural chemistry, fluoride incorporation also provides enhanced thermal stability of the oxide phases.

These observations encouraged us to investigate fluoride incorporation into oxovanadate−diphosphonate phases with more conventional cations, that is, organoammonium cations. In contrast to complex coordination cations, such as $\{Cu_2(bisterpy)\}^{4+}$ that bond to the surface oxo-groups of the V/P/O substructure to provide a complex bimetallic oxide framework, organoammonium cations assume charge-compensating, space-filling, and structure-directing roles through entrainment within vacancies in the V/P/O architecture. Consequently, removal of this organic component without collapse of the oxide substructure could provide a microporous material. This approach has allowed the synthesis and structural characterization of five members of this oxyfluorinated class of materials: the pillared layer phase $[H_2pip][V_4O_2F_4(H_2O)_2\ \{O_3P(CH_2)_3PO_3\}_2]$ (**1**), the two-dimensional (2D) phases $[H_2en][V_2O_2F_2(H_2O)_2\{O_3P(CH_2)_4PO_3\}]$ (**2**) and $[H_2en]_2[V_6F_{12}(H_2O)_2\{O_3P(CH_2)_5PO_3\}_2\{HO_3P(CH_2)_5PO_3H\}]$ (**3**), and the three-dimensional (3D) materials $[H_2en]_3[V_7O_6F_4(OH)_2\{O_3P(CH_2)_2PO_3\}_4]\cdot 7H_2O$ (**4**·$7H_2O$) and $(H_3O)[V_3F_2(H_2O)_2\ \{O_3P(CH_2)_2PO_3\}_2]\cdot 3.5H_2O$ (**5**·$3.5H_2O$) (pip = piperazine; en = ethylenediamine).

Experimental Section

General Considerations. All chemicals were used as obtained without further purification: vanadium (V) oxide, vanadyl sulfate hydrate, ammonium metavanadate, piperazine, ethylenediamine, diethylene triamine, and hydrofluoric acid (48−51%) were purchased from Aldrich; the diphosphonate ligands 1,2-ethylenediphosphonic acid, 1,3-propylenediphosphonic acid, 1,4-butylenediphosphonic acid, and 1,5-pentylenediphosphonic acid were prepared according to the literature method.[46] All syntheses were carried out in 23 mL poly(tetrafluoroethylene) lined stainless steel containers under autogenous pressure. The reactants were stirred briefly, and the initial pH was measured before heating. Water was distilled above 3.0 M Ω in-housing using a Barnstead model 525 biopure distilled water center. The reaction's initial and final pH were measured using Hydrion pH sticks.

Synthesis of $[H_2N(CH_2CH_2)_2NH_2][V_4O_2F_4(H_2O)_2\{O_3P(CH_2)_3PO_3\}_2]$ (1). A mixture of NH_4VO_3 (0.219 g, 1.872 mmol), 1,3-propylenediphosphonic acid (0.192 g, 0.941 mmol), H_2O (10.00 g, 556 mmol), piperazine (0.178 g, 1.433 mmol), and HF (0.350 mL, 10.14 mmol) in the mole ratio of 1.99:1.00:591:1.52:10.8 was stirred briefly before heating to 200 °C for 48 h. Initial and final pH values of 2.5 and 3.0, respectively, were recorded. Dark green crystals of **1** suitable for X-ray diffraction were isolated in 55% yield. IR (KBr pellet, cm^{-1}): 3410(b), 2931(w), 1617(m), 1508(w), 1466(w), 1401(w), 1257(m), 1068(m), 1025(s), 774(m), 724(m), 613(m). Anal. Calcd for $C_5H_{14}F_2NO_8P_2V_2$ (Found): F, 9.09 (8.50).

Synthesis of $[H_3N(CH_2)_2NH_3][V_2O_2F_2(H_2O)_2\{O_3P(CH_2)_4PO_3\}]$ (2). A solution of V_2O_5 (0.169 g, 0.929 mmol), 1,4-butylenediphosphonic acid (0.204 g, 0.929 mmol), H_2O (5.00 g, 278 mmol), ethylenediamine (0.085 mL, 1.265 mmol), and HF (0.250 mL, 7.25 mmol) in the mole ratio of 0.99:1.00:297:1.35:7.75 was stirred briefly before heating to 180 °C for 96 h (initial and final pH values were 2.0 and 2.0, respectively). Blue plates of **2** suitable for X-ray diffraction were isolated in 60% yield. IR (KBr pellet, cm^{-1}): 2941(w), 1618(m), 1560(m), 1458(w), 1398(w), 1330(w), 1206(m), 1103(m), 1081(m), 1035(s), 1009(m), 982(m), 797(m), 707(w).

Synthesis of $[H_3N(CH_2)_2NH_3]_2[V_6F_{12}(H_2O)_2\{O_3P(CH_2)_5PO_3\}_2\{HO_3P(CH_2)_5PO_3H\}]$ (3). A solution of V_2O_5 (0.170 g, 0.935 mmol), 1,5-pentylenediphosphonic acid (0.219 g, 0.944 mmol), H_2O (10.00 g, 556 mmol), ethylenediamine (0.085 mL, 1.265 mmol), and HF (0.300 mL, 8.70 mmol) with the mole ratio 1.01:1.00:595:1.35:9.30 was stirred briefly before heating to 200 °C for 96 h (initial and final pH of 2.0 and 2.0, respectively). Yellow plates of **3** were isolated in 45% yield, which were suitable for X-ray diffraction. IR (KBr pellet, cm^{-1}): 3409(b), 3224(w), 2942(w), 1636(w), 1541(w), 1489(m), 1407(w), 1303(w), 1194(w), 1076(s), 937(m), 799(w), 728(m). Anal. Calcd for $C_{9.5}H_{28}F_6N_2O_{10}P_3V_3$ (Found): F, 16.5 (15.8).

Synthesis of $[H_3N(CH_2)_2NH_3]_3[V_7O_6F_4(OH)_2\{O_3P(CH_2)_2PO_3\}_4]\cdot 7H_2O$ (4·$7H_2O$). A mixture of V_2O_5 (0.168 g, 0.924 mmol), 1,2-ethylenediphosphonic acid, (0.177 g, 0.931 mmol), H_2O (5.00 g, 278 mmol), ethylenediamine (0.085 mL, 1.265 mmol), and HF (0.200 mL, 5.80 mmol) in the mole ratio of 0.99:1.00:299:1.36:6.23 was heated to 180 °C for 72 h. Initial and final pH values of 2.0 and 2.0, respectively, were recorded. Blue crystals of **4**·$7H_2O$ suitable for X-ray diffraction were isolated in 70% yield. IR (KBr pellet, cm^{-1}): 3435(b), 3073(w), 2946(w), 2091(w), 1654(m), 1619(m), 1524(m), 1419(w), 1310(m), 1180(m), 1123(s), 1057(s), 966(m), 892(m), 725(m). Anal. Calcd. for $C_7H_{31}F_2N_3O_{19.5}P_4V_{3.5}$ (Found): F, 4.69 (5.03). Compound **4**·$7H_2O$ was heated at 350 °C to constant weight. The thermogravimetric analysis (TGA) and thermodiffractogram of this material indicated that the framework structure was retained upon dehydration and heating to constant weight. The dehydrated material **4′** gave elemental analyses consistent with the formulation $[NH_4][V_7O_7F_4\{O_3P(CH_2)_2PO_3\}_4]$. Anal. Calcd for $C_8H_{20}NO_{31}F_4P_8V_7$ (Found): C, 7.34 (7.80); H, 1.53 (1.56); N, 1.31 (1.07); F, 5.82 (6.34).

Synthesis of $[H_3O][V_3F_2(H_2O)_2\{O_3P(CH_2)_2PO_3\}_2]\cdot 3.5H_2O$ (5·$3.5H_2O$). A mixture of $VOSO_4$ (0.224 g, 1.37 mmol), 1,2-ethylenediphosphonic acid (0.174 g, 0.916 mmol), diethylene triamine (0.100 g, 0.969 mmol), H_2O (10.00 g, 556 mmol), and HF (0.350 mL, 10.14 mmol) with the mole ratio of 1.50:1.00:607:1.06:11.1. The mixture was stirred briefly before heating to 100 °C for 48 h with an initial and final pH of 1.5 and 1.5, respectively. Black crystals of **5**·$3.5H_2O$ suitable for X-ray diffraction were isolated in 75% yield. IR (KBr pellet, cm^{-1}): 3400(b), 1637(m), 1509(m), 1459(w), 1420(w), 1196(m), 990(s), 750(m), 511(m). Anal. Calcd for $C_2H_9FO_{9.25}P_2V_{1.5}$ (Found): F, 5.61 (4.33).

X-ray Crystallography. Structural measurements for **1**−**5** were performed on a Bruker-AXS SMART-CCD diffractometer at low temperature (90 K) using graphite-monochromated Mo Kα radiation ($\lambda_{MoK\alpha}$ = 0.71073 Å).[47] The data were corrected for Lorentz and polarization effects and absorption using SADABS.[48] The structures were solved by direct methods. All non-hydrogen atoms were refined anisotropically. After all of the non-hydrogen atoms were located, the models were refined against F^2 by initially using isotropic and later anisotropic thermal displacement parameters.

(46) Arnold, D. I.; Ouyang, X.; Clearfield, A. *Chem. Mater*. **2002**, *14*, 2020.

(47) *SMART Software*, Version 5.630; Siemens Analytical X-ray Instruments, Ins.; Bruker-AXS: Madison, WI, 1994.

(48) Sheldrick, G. M. *SADABS: Program for Empirical Absorption Corrections:* University of Göttingen: Göttingen, Germany, 1996.

Table 1. Summary of Crystallographic Data for the Structures of **1**, **2**, **3**, **4**·$7H_2O$, and **5**·$H_3O(H_2O)_{3.5}$

	1	**2**	**3**	**4**·$7H_2O$	**5**·$H_3O(H_2O)_{3.5}$
empirical formula	$C_5H_{14}F_2NO_8P_2V_2$	$C_6H_{22}F_2N_2O_{10}P_2V_2$	$C_{9.5}H_{28}F_6N_2O_{10}P_3V_3$	$C_7H_{31}F_2N_3O_{19.5}P_4V_{3.5}$	$C_2H_9FO_{9.25}P_2V_{1.5}$
fw	417.99	484.08	690.07	809.52	338.44
cryst syst	monoclinic	monoclinic	triclinic	triclinic	monoclinic
space group	$P2_1/n$	$C2/c$	$P\bar{1}$	$P\bar{1}$	$P2/m$
a (Å)	7.561(2)	28.836(3)	7.8942(8)	9.0982(5)	7.1564(6)
b (Å)	14.189(3)	5.3256(5)	9.3578(9)	11.8549(6)	18.227(2)
c (Å)	11.174(2)	10.245(1)	17.202(2)	12.0113(7)	8.1397(7)
α (deg)	90	90	99.6552(2)	103.128(1)	90
β (deg)	99.04(3)	95.051(2)	96.062(2)	90.775(1)	95.038(2)
γ (deg)	90	90	107.762(2)	91.887(1)	90
V (Å^3)	1183.9(4)	1567.2(3)	1330.6(2)	1260.7(1)	1057.6(2)
Z	4	8	2	2	4
D_{calcd} (g cm^{-3})	2.345	2.052	1.948	2.133	2.126
μ (mm^{-1})	1.915	1.473	1.467	1.624	1.702
T (K)	90	90	90	90	90
λ (Å)	0.71073	0.71073	0.71073	0.71073	0.71073
R1[a]	0.0404	0.0449	0.0620	0.0516	0.0595
wR2[b]	0.0843	0.0974	0.1294	0.1211	0.1304

[a] $R1 = \sum||F_o| - |F_c||/\sum|F_o|$. [b] $wR2 = \{\sum[w(F_o^2 - F_c^2)^2]/\sum[w(F_o^2)^2]^{1/2}\}$; $w = 1/[\sigma^2(F_o^2) + (aP)^2 + bP]$; $P = [\mathrm{Max}(F_o^2,0) + 2F_c^2]/3$.

Hydrogen atoms were introduced in calculated positions and refined isotropically. Scattering coefficients and anomalous dispersion corrections of neutral atoms were taken from the *International Tables*, Vol. C. All calculations were performed using SHELXTL crystallographic software packages.[49] Crystallographic details for structures **1**−**5** are summarized in Table 1. Space group assignments and structure solutions and refinements were unexceptional except for compound **5**. Compound **5** was determined to be nonmerohedrally twinned from the initial diffraction pattern. The program *Cell_Now*[50] indicated that compound **5** was composed of two crystal domains with the second domain rotated by 180° with respect to the first crystal domain. A twin law was created and imported into SAINT-Plus software package[51] where the data were corrected for Lorentz and polarization effects and absorption using TWINABS.[52] The structure then was solved by direct methods and refined by the conventional methodology.

Atomic positional parameters, full tables of bond lengths and angles, and anisotropic temperature factors are available in the Supporting Information. Selected bond lengths and angles for **1**−**5** are given in Tables 2−6.

Magnetism. Magnetic data were recorded on 17−25 mg samples of compound in the 2−300 K temperature range using a Quantum Design MPMS-5S superconducting quantum interference device (SQUID) spectrometer. Calibrating and operating procedures have been reported previously.[53] The temperature-dependent data were obtained at a magnetic field of **H** = 1000 Oe.

Thermal Gravimetric Analyses. Thermogravimetric studies were performed using 10−25 mg samples in an Auto TGA (thermogravimetric analysis) 2950 instrument under a 50 mL/min flow of synthetic air. The temperature was ramped from 25 to 650 °C at a rate of 5 °C/min for the decomposition.

Thermodiffraction. Thermodiffraction data were collected on a Bruker-AXS D8 Advance automated diffractometer equipped with a TTK 450 heating stage using Cu Kα radiation. The powder was placed in the sample holder, which acted as the heating system. The step size was 0.02° in 2θ, and the heating rate from room temperature to 275 °C was 0.5 and 0.2 °C/s for the temperature range 300−425 °C. The delay time between reaching the set temperature and measuring the diffraction pattern was 5 min. All temperature spectra were collected under a vacuum.

Table 2. Selected Bond Lengths (Å) and Angles (deg) for **1**[a]

V(1)−O(3)	1.614(2)	O(4)−V(1)−F(1)	155.09(9)
V(1)−O(4)	1.961(2)	O(2)−V(1)−O(5)	165.86(9)
V(1)−O(2)	1.978(2)	O(3)−V(1)−F(2)	166.81(9)
V(1)−F(1)	2.017(2)	F(2)−V(2)−O(1)	172.86(9)
V(1)−O(5)	2.030(2)	O(6)−V(2)−O(7)	174.6(1)
V(1)−F(2)	2.281(2)	F(1)−V(2)−O(90)	173.3(1)
∑vs	3.93		
V(2)−F(2)	1.913(2)		
V(2)−O(6)	1.931(2)		
V(2)−O(1)	1.942(2)		
V(2)−O(7)	1.969(2)		
V(2)−F(1)	1.988(2)		
V(2)−O(90)	2.126(3)		
∑vs	3.11		

[a] ∑vs refers to the bond-valence sums for the vanadium atoms, which are calculated using Brese, N. E.; O'Keeffe, M. *Acta Crystallogr. Sect. B* **1991**, *47*, 192.

Table 3. Selected Bond Lengths (Å) and Angles (deg) for **2**[a]

V(1)−O(3)	1.590(2)	O(4)−V(1)−O(1)	165.48(8)
V(1)−O(5)	2.002(2)	O(5)−V(1)−O(2)	158.31(8)
V(1)−O(4)	2.027(2)	O(3)−V(1)−F(1)	176.90(9)
V(1)−O(1)	2.035(2)		
V(1)−O(2)	2.062(2)		
V(1)−F(1)	2.162(1)		
∑vs	4.03		

[a] ∑vs refers to the bond-valence sums for the vanadium atoms, which are calculated using Brese, N. E.; O'Keeffe, M. *Acta Crystallogr. Sect. B* **1991**, *47*, 192.

Results and Discussion

Synthesis and Spectroscopy. The bimetallic oxides of this study were prepared by conventional hydrothermal methods,[54−57] which, as noted, provide ideal conditions for

(49) Sheldrick, G. M. *SHELXTL-Plus: Program for Refinement of Crystal Structures*, Version 6.14; Bruker-AXS: Madison, WI, 1996.
(50) Sheldrick, G. M. *Cell_Now*, 1−22−2204; Bruker-AXS: Göttingen, Germany, 2004.
(51) Sheldrick, G. M. *SAINT-Plus*, Version 6.45; Bruker-AXS: Madison, WI, 1996.
(52) Sheldrick, G. M. *TWINABS: Program for the Empirical Absorption Corrections for Twins*; Bruker-AXS: Madison, WI, 2003.
(53) O'Connor, C. J. *Prog. Inorg. Chem.* **1979**, *29*, 203−283.
(54) Whittingham, M. S. *Curr. Opin. Solid State Mater. Sci.* **1996**, *1*, 227.
(55) Laudise, R. A. *Chem. Eng. News* **1987**, *65*, 30.

Table 4. Selected Bond Lengths (Å) and Angles (deg) for **3**[a]

V(1)−F(1)	1.909(3)	F(1)−V(1)−O(4)	172.6(2)
V(1)−O(1)	1.951(3)	O(1)−V(1)−F(3)	174.4(1)
V(1)−O(4)	1.970(4)	F(2)−V(1)−O(2)	175.4(2)
V(1)−F(3)	1.979(3)	F(4)−V(2)−O(5)	166.2(2)
V(1)−F(2)	2.004(3)	F(3)−V(2)−F(5)	179.0(1)
V(1)−O(2)	2.015(4)	O(6)−V(2)−O(90)	175.2(2)
∑vs	3.08	F(6)−V(3)−O(7)	171.9(2)
V(2)−F(4)	1.839(3)	F(2)−V(3)−O(8)	178.9(2)
V(2)−O(6)	1.931(4)	O(9)−V(3)−F(5)	177.1(1)
V(2)−O(5)	1.974(4)		
V(2)−F(3)	1.988(3)		
V(2)−F(5)	2.007(3)		
V(2)−O(90)	2.130(5)		
∑vs	3.08		
V(3)−F(6)	1.909(3)		
V(3)−O(7)	1.961(3)		
V(3)−F(2)	1.988(3)		
V(3)−O(9)	2.002(4)		
V(3)−O(8)	2.005(4)		
V(3)−F(5)	2.007(3)		
∑vs	3.01		

[a] ∑vs refers to the bond-valence sums for the vanadium atoms, which are calculated using Brese, N. E.; O'Keeffe, M. *Acta Crystallogr. Sect. B* **1991**, *47*, 192.

Table 5. Selected Bond Lengths (Å) and Angles (deg) for **4**·$7H_2O$[a]

V(1)−O(1)	1.599(3)	F(1)−V(1)−O(3)	159.6(1)
V(1)−F(1)	1.955(2)	O(2)−V(1)−O(4)	159.2(1)
V(1)−O(3)	1.968(3)	O(1)−V(1)−F(1)	179.1(1)
V(1)−O(2)	2.014(3)	O(8)−V(2)−O(6)	178.1(1)
V(1)−O(4)	2.019(3)	O(5)−V(2)−O(9)	174.6(1)
V(1)−F(1)	2.187(2)	O(7)−V(2)−O(11)	178.6(1)
∑vs	4.09	O(11)−V(3)−O(11)	180.0
V(2)−O(7)	1.863(3)	O(12)−V(3)−O(12)	180.0
V(2)−O(5)	1.956(3)	O(10)−V(3)−O(10)	180.0
V(2)−O(8)	1.957(3)	O(16)−V(4)−O(15)	159.8(1)
V(2)−O(6)	1.963(3)	F(2)−V(4)−O(13)	159.2(1)
V(2)−O(9)	1.979(3)	O(14)−V(4)−F(2)	176.4(1)
V(2)−O(11)	2.047(3)		
∑vs	3.69		
V(3)−O(11)	1.886(3)		
V(3)−O(11)	1.886(3)		
V(3)−O(12)	1.992(2)		
V(3)−O(12)	1.992(2)		
V(3)−O(10)	1.999(2)		
V(3)−O(10)	1.999(2)		
∑vs	3.71		
V(4)−O(14)	1.604(3)		
V(4)−F(2)	1.957(2)		
V(4)−O(16)	1.997(3)		
V(4)−O(15)	2.008(3)		
V(4)−O(13)	2.011(3)		
V(4)−F(2)	2.164(2)		
∑vs	4.05		

[a] ∑vs refers to the bond-valence sums for the vanadium atoms, which are calculated using Brese, N. E.; O'Keeffe, M. *Acta Crystallogr. Sect. B* **1991**, *47*, 192.

solubilizing and crystallizing organic/inorganic hybrid materials.[58] For compounds **1**−**5**, the reaction mixture consists of a vanadate source, a diphosphonate ligand, an organoammonium cation, and HF with reaction times of 48−96 h at temperatures of 180−200 °C. While HF is conventionally

Table 6. Selected Bond Lengths (Å) and Angles (deg) for **5**·$3.5H_2O$[a]

V(1)−O(2)	1.954(3)	O(2)−V(1)−O(2)	180.0
V(1)−O(2)	1.954(3)	O(2)−V(1)−O(2)	180.0
V(1)−O(2)	1.954(3)	O(1)−V(1)−O(1)	180.0
V(1)−O(2)	1.954(3)	F(2)−V(2)−F(1)	179.42(13)
V(1)−O(1)	1.967(5)	O(6)−V(2)−O(4)	178.08(15)
V(1)−O(1)	1.967(5)	O(3)−V(2)−O(5)	179.72(16)
∑vs	3.25	O(8)−V(3)−O(8)	180.0
V(2)−F(2)	1.942(2)	O(7)−V(3)−O(7)	180.0
V(2)−O(6)	1.963(3)	O(7)−V(3)−O(7)	180.0
V(2)−O(3)	1.963(3)		
V(2)−F(1)	1.973(1)		
V(2)−O(4)	1.976(3)		
V(2)−O(5)	1.984(3)		
∑vs	3.16		
V(3)−O(8)	1.848(4)		
V(3)−O(7)	1.861(5)		
V(3)−O(7)	1.861(5)		
V(3)−O(7)	2.041(8)		
V(3)−O(7)	2.041(8)		
V(3)−O(8)	2.30(2)		
∑vs	3.22		

[a] ∑vs refers to the bond-valence sums for the vanadium atoms, which are calculated using Brese, N. E.; O'Keeffe, M. *Acta Crystallogr. Sect. B* **1991**, *47*, 192.

introduced as a mineralizer to influence solubility and crystal growth and is not incorporated into the product, oxyfluorinated products have been reported previously for hybrid materials of the vanadium and molybdenum oxides.[59−62] In this case, it was observed that at low HF/V molar ratios (0.5:1 or less) the products were of the general class (organoammonium cation)$[V_xO_y(O_3PR)_z]$ and exhibited no fluoride incorporation. In contrast, increased HF:V ratios (3:1−10:1) provided the oxyfluoride materials of this study.

Although V(V) starting materials were employed in the syntheses of **1**−**4**, the products contained only reduced vanadium, that is, exclusively V(IV) in **2** and **4**, V(III) in **3**, and mixed valence V(IV)/V(III) in **1**. Similarly, while the V(IV) starting material $VOSO_4$ is used in the preparation of **5**, the product contains exclusively V(III). Reduction of vanadium in the presence of nitrogenous compounds under hydrothermal conditions is not unusual. However, reduction to V(III) is only common in the presence of fluoride and particularly with excess fluoride and concomitant fluoride incorporation.

While ethylenediammonium and piperazinium cations were incorporated as charge-compensating units, the more sterically demanding diethylenetriamine was not entrained in the structure of **5** in which charge-compensation is provided by a hydronium cation, which is in contrast to structures **1**−**4**.

The infrared spectra of **1**−**5** are characterized by a series of three or four bands in the 1000−1650 cm^{-1} range, which is attributed to the diphosphonate ligand. Curiously, the oxyfluorinated materials do not exhibit a bond readily assigned to υ(V═O).

Crystal Structures. As shown in Figure 1b, the structure of **1** exhibits the characteristic pillared layer structure, with

(56) Lobachev, A. N. *Crystallization Processes Under Hydrothermal Conditions*; Consultants Bureau, New York, 1973.
(57) Gopalakrishnan, J. *Chem. Mater.* **1995**, *7*, 1265.
(58) Zubieta, J. Solid-State Methods, Hydrothermal. In *Comprehensive Coordination Chemistry II;* McCleverty, J. A., Meyer, T. J.; Elsevier Science: New York, 2004; Vol. 1, pp 697−709.
(59) Riou, D.; Férey, G. *J. Solid State Chem.* **1994**, *111*, 422.
(60) Ninclaus, C.; Riou, D.; Férey, G. *Chem. Commun.* **1997**, 851.
(61) Burkholder, E.; Zubieta, J. *Inorg. Chim. Acta* **2004**, *357*, 279.
(62) Burkholder, E.; Golub, V.; O'Connor, C. J.; Zubieta, J. *Inorg. Chem.* **2004**, *43*, 7014.

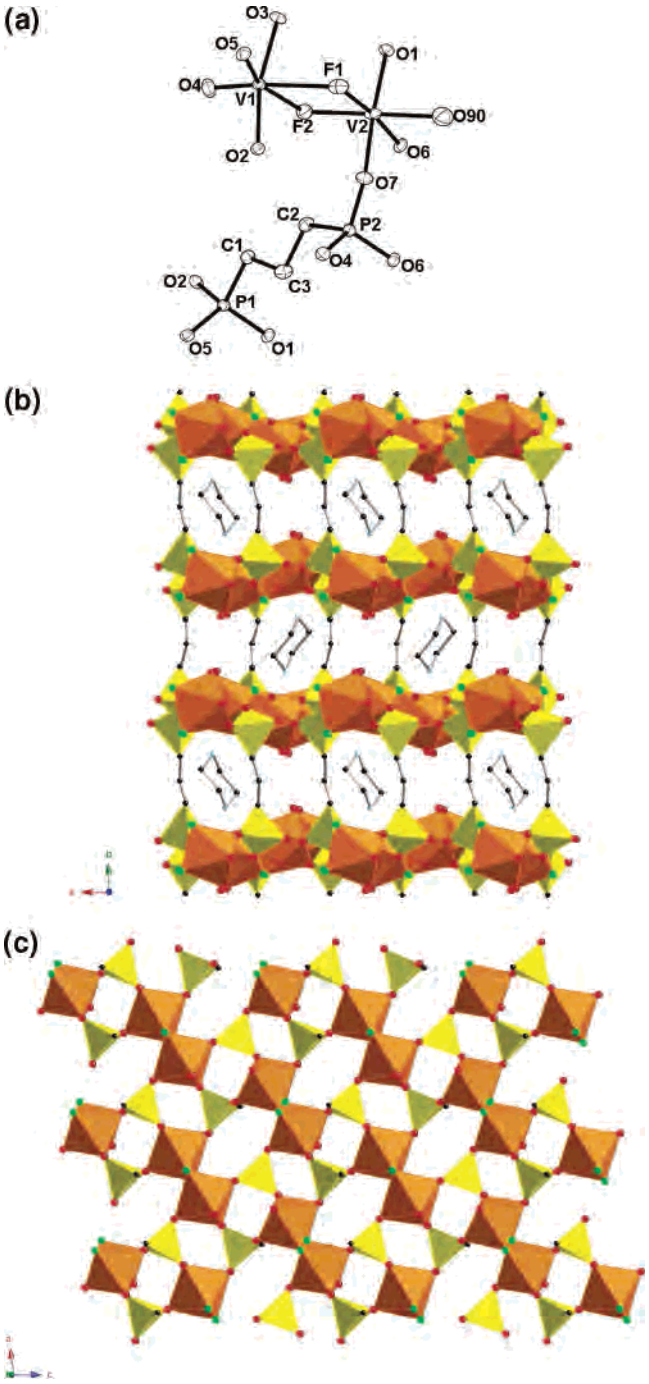

Figure 1. (a) An ORTEP view of the structure of **1** showing the atom-labeling scheme and 50% thermal ellipsoids. (b) A polyhedral representation of the structure of **1** viewed parallel to the crystallographic *a* axis. (c) A view of the V/P/O/F network of **1** in the *ac* plane. The elements are represented by the following color scheme: vanadium, orange polyhedra; phosphorus, yellow polyhedra; oxygen, red spheres; fluorine, green spheres; nitrogen, light blue spheres; carbon, black spheres.

$[V_4O_2F_4(H_2O)_2\{O_3P(CH_2)_3PO_3\}_2]_n^{2n-}$ layers buttressed by the propylene bridges of the diphosphonate ligands. The piperazinium cations reside in large galleries between the inorganic layers and are bounded by the propylene chains. The V/O/F/P inorganic network substructure (Figure 1c) is constructed from corner-sharing phosphorus tetrahedra and corner- and edge-sharing vanadium octahedra. The vanadium component is present as edge-sharing pairs of octahedra with each one linked through six phosphorus tetrahedra to six adjacent binuclear units. One vanadium site of each binuclear unit is V(IV) with a terminal oxo-group, two bridging fluorides, and three phosphonate oxygen donors defining the coordination geometry, while the second is V(III) with an aqua ligand replacing the oxo-group of the V(IV) site.

Each $\{V_2O_{10}F_2\}$ binuclear unit is linked to six phosphorus tetrahedra that bridge the unit to six adjacent binuclear building blocks. Each $\{PO_3\}$ terminus of the diphosphonate ligands bridges three binuclear oxyfluorovanadate clusters. This connectivity pattern results in four and six polyhedra connect rings, that is, $\{V_2P_2O_4\}$ and $\{V_4P_2O_4F_2\}$ heterocycles.

The propylene tethers of the diphosphonate ligands project from either face of the V/P/O/F layers to provide connectivity between adjacent layers with an interlayer separation of 8.1 Å. The piperazinium cations occupy large galleries in the interlamellar domain of approximate dimensions 11.2 × 7.3 Å. The cations engaged in hydrogen bonding to the phosphonate groups of the layers (N1···O5, 2.849(5) Å).

In contrast to the overall 3D structure of **1**, **2** exhibits a 2D structure (Figure 2b) that is constructed from pairs of V/P/O/F layers linked through the butyl chains of the diphosphonate ligands into slabs of 11.9 Å thickness with the $[H_3NCH_2CH_2NH_3]^{2+}$ cations separating adjacent slabs. The inorganic network is constructed from mononuclear V(IV) octahedra linked through corner-sharing phosphorus tetrahedra. The vanadium coordination geometry is defined by a terminal oxo-group, an aqua ligand, a terminal fluoride, and three oxygen donors from phosphonate ligands. The oxo-group projects into an intralamellar cavity, while the aqua ligand projects into the slab interior. The fluoride groups are directed from either face of the slab into the interlamellar regions.

Within the V/P/O/F layers, each $\{VO_5F\}$ octahedron engages in corner-sharing with three phosphonate tetrahedron and each bridges three adjacent vanadium sites. Thus, each vanadium octahedron is linked through phosphorus tetrahedra to six adjacent octahedra in the layer. The connectivity pattern generates six polyhedral connect or $\{V_3P_3O_6\}$ rings. As shown in Figure 2c, the layer structure may be described as a defected $MO(PO_4)$ network,[63−67] which results from the substitution of a {P−O} linkage with a terminal aqua ligand at each vanadium site, and the unavailability of the fourth vertex at each phosphorus for in-plane linking to the vanadium sites. In other words, one shared tetrahedral vertex at each vanadium site of the $MO(PO)_4$ prototype is replaced by an aqua ligand in **2**.

The cations occupy the interslab domain and engage in hydrogen bonding to the fluorines of the layers with N···F distances of 2.645(4) Å. The spacing between slabs is 4.09

(63) Longo, J. M.; Kierkegaard, P. *Acta Chem. Scand.* **1966**, *20*, 72.
(64) Longo, J. M.; Pierce, J. W.; Kafalas, J. A. *Mater. Res. Bull.* **1971**, *6*, 1157.
(65) Eick, H. A.; Kihlborg, L. *Acta Chem. Scand.* **1966**, *20*, 722.
(66) Kierkegaard, P.; Westerlund, M. *Acta Chem. Scand.* **1964**, *18*, 2217.
(67) Finn, R. C.; Zubieta, J.; Haushalter, R. C. *Prog. Inorg. Chem.* **2003**, *51*, 421.

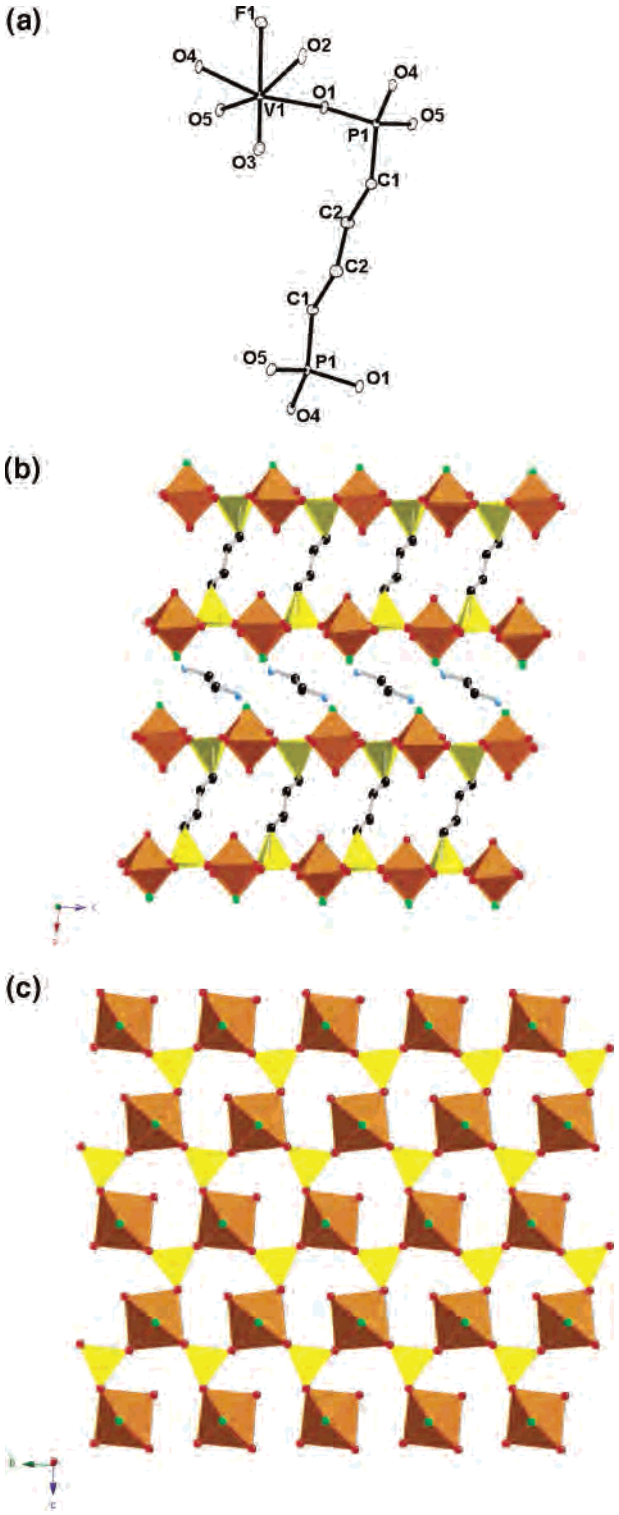

Figure 2. (a) An ORTEP view of the structure of **2** showing the atom-labeling scheme and 50% thermal ellipsoids. (b) A polyhedral view of the structure of **2** viewed parallel to the crystallographic *b* axis. (c) The V/P/O/F network of **2** in the *bc* plane. The elements are represented by the following color scheme: vanadium, orange polyhedra; phosphorus, yellow polyhedra; oxygen, red spheres; fluorine, green spheres; nitrogen, light blue spheres; carbon, black spheres.

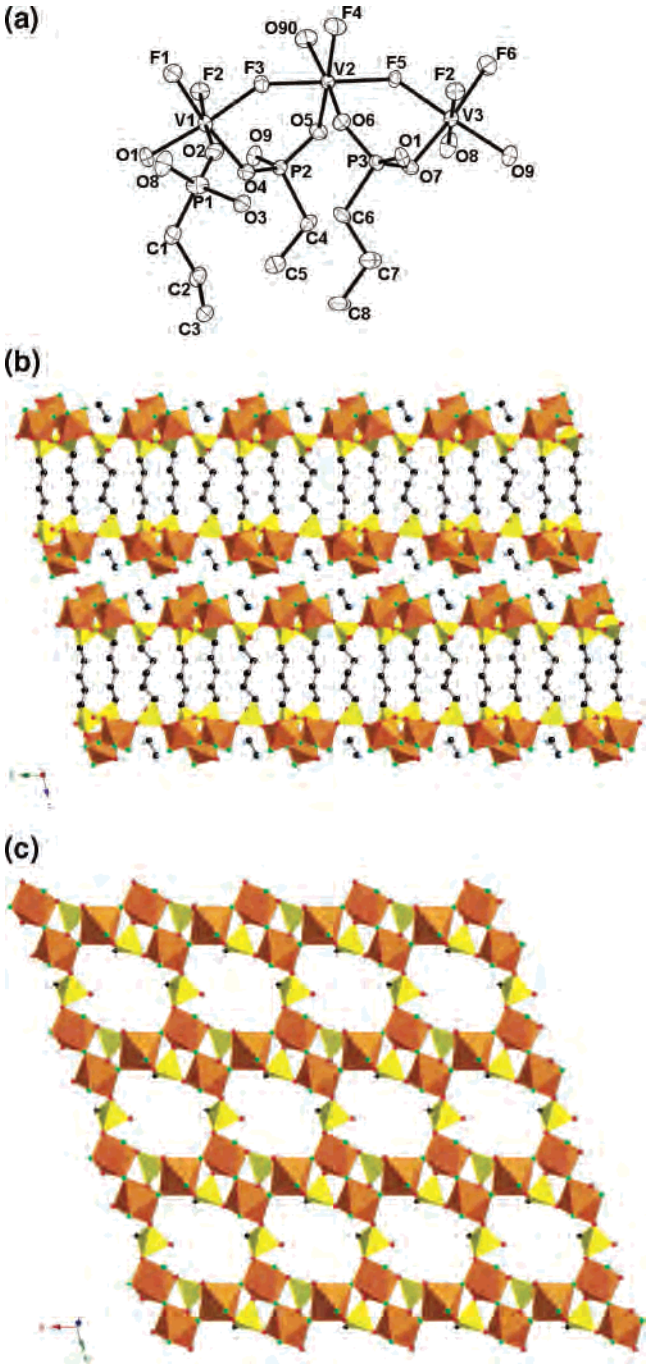

Figure 3. (a) An ORTEP representation of the structure of **3** illustrating the atom-labeling scheme and 50% thermal ellipsoids. (b) A view of the structure of **3** parallel to the crystallographic *a* axis. (c) The V/P/O/F network of **3** in the *ab* plane. The elements are represented by the following color scheme: vanadium, orange polyhedra; phosphorus, yellow polyhedra; oxygen, red spheres; fluorine, green spheres; nitrogen, light blue spheres; carbon, black spheres.

Å, which results in alternation of repeat distances along the crystallographic *a* axis.

The structure of **3**, which is shown in Figure 3b, is similar to **2** because it also consists of 2D slabs constructed from two V/P/O/F networks buttressed by the pentyl tethers of the diphosphonate ligands. The distance between the V/P/O/F faces of a slab is 16.1 Å, while the distance between the faces of adjacent slabs along the *c* axis is 3.18 Å. The $[H_3NCH_2CH_2NH_3]^{+2}$ cations occupy the interlamellar domain.

In contrast to the network substructure of **2**, the network substructure of **3** (Figure 3c) consists of chains of corner-

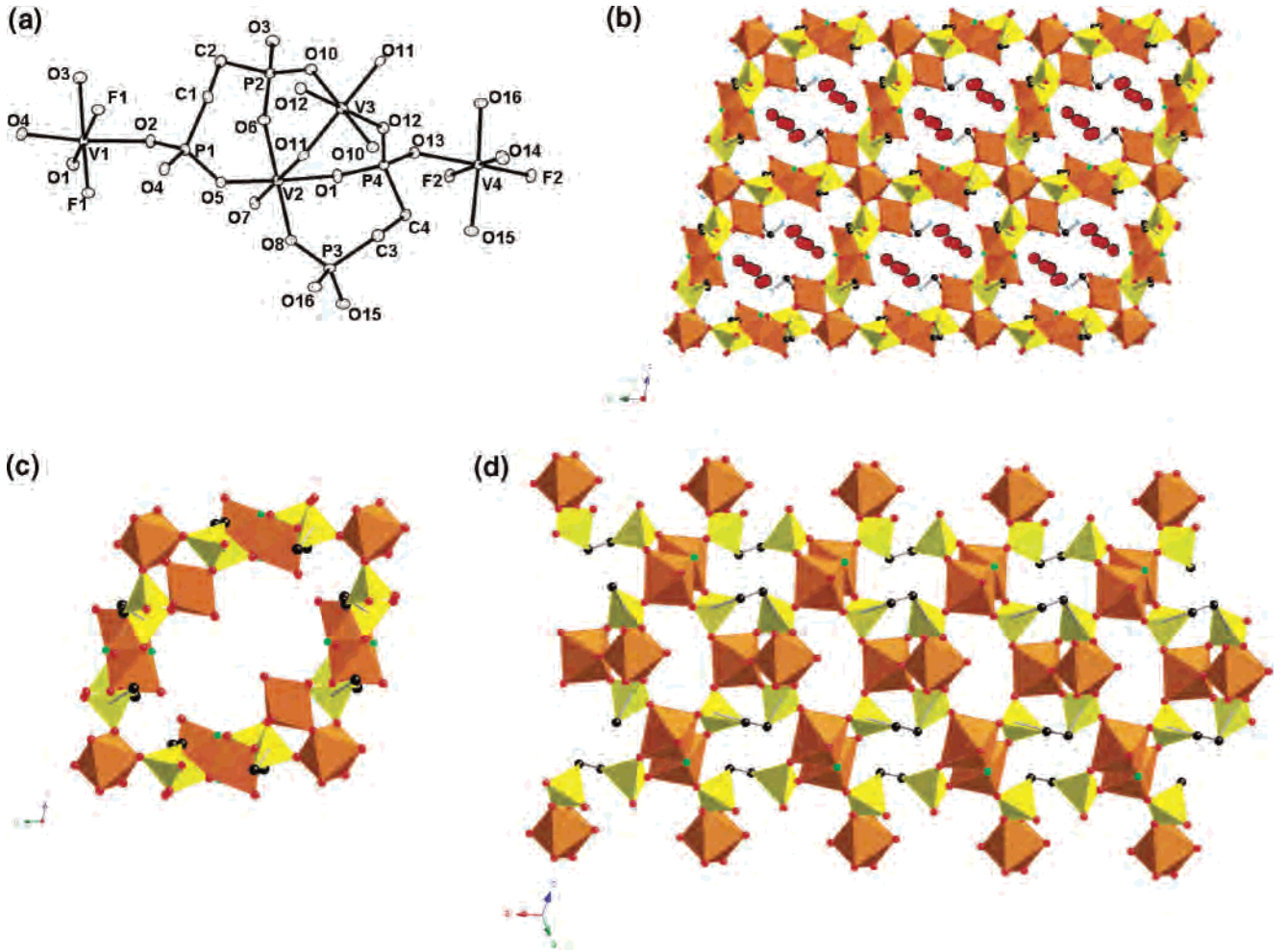

Figure 4. (a) An ORTEP representation of the structure of **4**·7H_2O (50% thermal ellipsoids). (b) A polyhedral representation of the structure of **4** viewed parallel to the *a* axis and showing the cavities occupied by the water of crystallization. (c) A view of the $[V_6F_7O_6\{O_3P(CH_2)_2PO_3\}_4]_n^{4n-}$ network substructure of **4**. The elements are represented by the following color scheme: vanadium, orange polyhedra; phosphorus, yellow polyhedra; oxygen, red spheres; fluorine, green spheres; nitrogen, light blue spheres; carbon, black spheres.

sharing V(III) octahedra linked through phosphorus tetrahedra. The zigzag vanadium chain contains two distinct V(III) environments. The first is defined by a terminal fluoride, two bridging fluorides, and three phosphonate oxygen donors, while the second site exhibits a terminal and two bridging fluorides, two phosphonate oxygen donors, and an aqua ligand that projects into the interlamellar region. In common with the structure of **2**, the fluoride ligands of **3** are disposed on the outer surfaces of the slabs, that is, directed toward the interlamellar domain.

There are two distinct diphosphonate environments. Either $\{O_3P\}$ terminus of the first engages in corner-sharing with three adjacent vanadium sites of a chain to produce the pronounced puckering of the layer in the *bc* plane. The phosphorus termini of the second diphosphonate ligand share vertices with vanadium sites of two adjacent chains in a slab and exhibit a pendant $\{P-OH\}$ group. This polyhedral connectivity pattern generates three polyhedron connects or $\{V_2PO_3\}$ rings and larger 10-connect or 20-membered $\{V_6P_4O_{10}\}$ rings. The $\{P-OH\}$ residues are directed into these large intralamellar void spaces and tilted into the organic domain sandwiched between the inorganic layers of the slab.

The folding of the V/P/O/F layers orients the vanadium polyhedra on the outer faces of the slabs while directing the phosphorus tetrahedra toward the inner faces. One consequence of this arrangement of polyhedra is that it produces a shallow sinusoidal profile to the inorganic layers with an amplitude of 3.35 Å, and a period of 9.28 Å when viewed along the *a* axis. This ruffling of the surfaces of the layers produces hollows at either face of the inorganic slab. Consequently, neighboring slabs achieve close proximity by aligning hollows and projecting vanadium polyhedra. The cations nestle within the hollows and are hydrogen bonded to the layers with N2···F6, N1···O5, and N1···LO6 distances of 2.732(5), 3.126(5), and 3.184(5) Å, respectively.

The structural consequences of shortening the diphosphonate tether length are manifested in the 3D structure of **4**·7H_2O shown in Figure 4b. The structure of **4** does not conform to the pillared layer prototype but rather exhibits 3D V/O/F/P connectivity that produces large 16-connect channels, which encapsulate large amounts of water of crystallization as well as the cations. There are two distinct V(IV) building blocks. The first is a trinuclear unit of corner-sharing octahedra that consist of a disordered

$\{V_3O_2(H_2O)_2\}^{8+}$ chain linked through four diphosphonate ligands to eight adjacent binuclear vanadyl subunits. The central vanadium of the triad corner-shares with four phosphorus tetrahedra in the equatorial plane with the trans axial positions occupied by bridging oxo-groups. The peripheral vanadium sites of the trinuclear unit exhibits geometries defined by four oxygen donors from the diphosphonate ligands in the equatorial plane, which has a bridging oxo-group and an aqua ligand, that projects into the large cavities in the axial positions. The binuclear sites exhibit edge-sharing through a pair of fluoride bridges with the remaining coordination sites in each case accommodating a terminal oxo-group and three phosphonate oxygen donors.

Each diphosphonate ligand adopts a relatively unusual chelating mode to one peripheral vanadium site of the triad, forming a {V−O−P−C−C−P−O-} ring. Another oxygen vertex of one phosphorus terminus of the diphosphonate is shared with the central vanadium site of the trinuclear unit. The three remaining oxygen vertices of each diphosphonate unit bridge to two binuclear vanadate subunits. Each trinuclear unit coordinates to four diphosphonate ligands and, consequently, is tethered through the diphosphonates to eight adjacent binuclear subunits.

As shown in Figure 4c, the structure may be alternatively described as $\{V_6F_7O_6\{O_3P(CH_2)_2PO_3\}_4\}_n^{4n-}$ layers linked through the central vanadium sites of the trinuclear subunit. The layer is constructed from eight polyhedral connects or $\{V_4P_4O_8\}$ rings. The diphosphonate ligands bridge adjacent rings, which also are fused at the common V2 sites so as to produce daisy chains of rings running parallel to the *a* axis. Adjacent chains are linked through the binuclear vanadium units.

The large framework cavities encapsulate the water of crystallization and the $[H_3NCH_2CH_2NH_3]^{2+}$ cations, which are hydrogen-bonded to the inorganic substructure with N1···O6 and N2···O8 distances of 2.889(6) and 2.894(6) Å, respectively.

As shown in Figure 5b, the structure of **5**·4.3H_2O may be described as pillared layers but with octahedral $\{VO_6\}$ units providing the pillaring for $[V_2F_2\{O_3P(CH_2)_2PO_3\}_2]_n^{4n-}$ networks. The networks (Figure 5c) are constructed from chains of corner-sharing V(III) octahedra linked through phosphorus tetrahedra. The vanadium sites of the chain exhibit trans bridging fluorides and four oxygen donors from phosphonate ligands. The mononuclear V(III) pillaring site exhibits trans aqua ligands and four phosphonate oxygen donors. One diphosphonate subunit links two chains and one pillaring vanadium site, while the second bridges two chains and two pillaring sites. When the structure is viewed parallel to the *a* axis, it is apparent that the polyhedral connectivity pattern produces two distinct water-filled channels with one bordered by four vanadium and four phosphorus polyhedra in a $\{V_4P_4O_8\}$ ring, and the second with a perimeter defined by two vanadium polyhedra and two diphosphonate ligands in a $\{V_2P_4O_4C_4\}$ ring.

General Structural Observations. In common with the previously described oxyfluorovanadium/copper-bisterpy/organodiphosphonate system,[45] the structural chemistry of the oxyfluorovanadium/organodiphosphonate materials of this study reveals the absence of a persistent V−P−O(F)

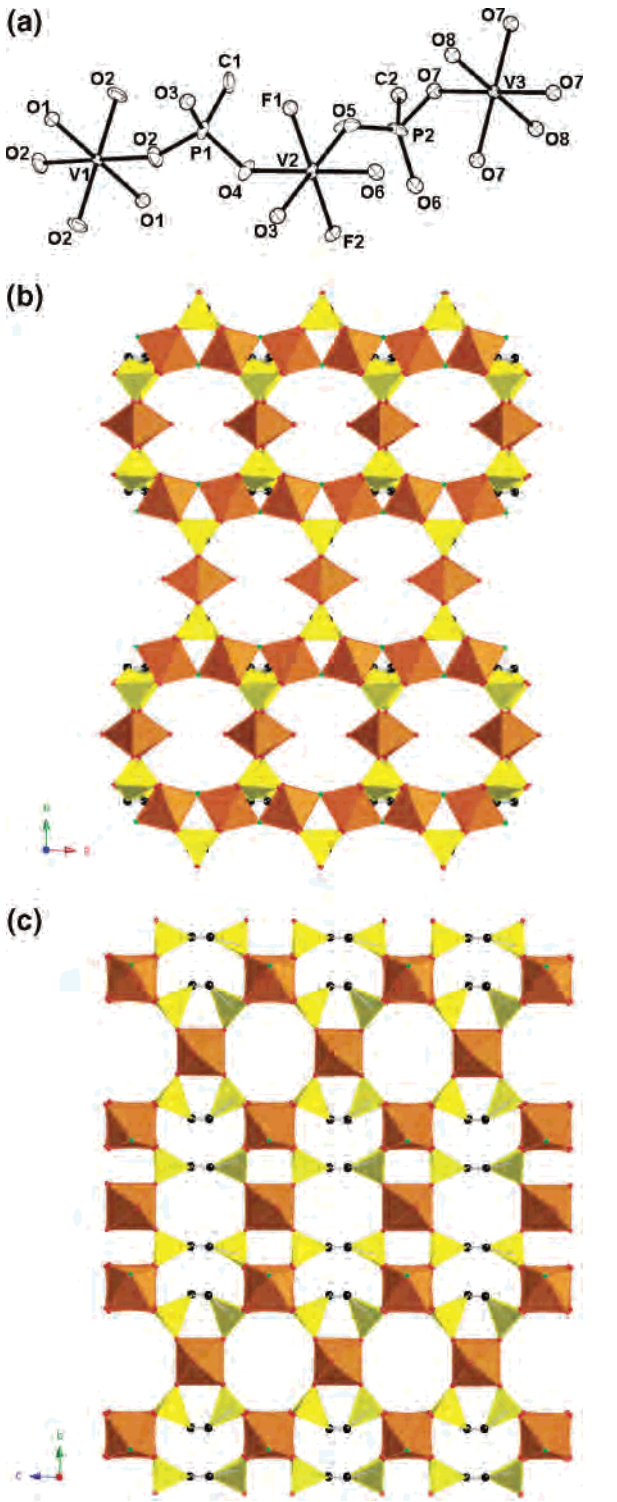

Figure 5. (a) An ORTEP view of the structure of **5**·3.5H_2O showing the atom-labeling scheme and 50% thermal ellipsoids. (b) A polyhedral representation of the structure of **5**, viewed parallel to the crystallographic *c* axis. (c) The $[V_2F_2\{O_3P(CH_2)_2PO_3\}_2]_n^{4n-}$ substructure of **5** viewed in the *bc* plane. The elements are represented by the following color scheme: vanadium, orange polyhedra; phosphorus, yellow polyhedra; oxygen, red spheres; fluorine, green spheres; nitrogen, light blue spheres; carbon, black spheres.

Table 7. A Comparison of Selected Structural Characteristics and Component Building Blocks of $V_xO_yF_z$/Organophosphonates

compound	overall dimensionality	vanadium building blocks	inorganic substructure: V/P/O/F or Cu/V/P/O/F	V−X−V linkages	ref
1	3D	binuclear units of edge-sharing V(IV) and V(III) octahedra	$\{V_2OF_2(H_2O)(O_3P\text{-})_2\}_n^{n-}$ layers	$\{V_2F_2\}$	this work
2	2D	octahedra	$\{VOF(H_2O)(O_3P\text{-})\}_n^{n-}$ layers	no	this work
3	2D	chains of corner-sharing V(III) octahedra	$\{V_3F_6(H_2O)(O_3P\text{-})_2(HO_3P\text{-})\}_n^{2n-}$ layers	V−F−V	this work
4	3D	trinuclear units of corner-sharing V(IV) octahedra, binuclear units of edge-sharing V(IV) octahedra	$\{V_7O_6F_4(H_2O)_2(O_3P\text{-})_8\}_n^{4n-}$ 3D framework	V−O−V and $\{V_2F_2\}$	this work
5	3D	chains of edge-sharing V(III) octahedra; isolated V(III) octahedra	$\{V_3F_2(H_2O)_2(O_3P\text{-})_4\}_n^{n-}$ 3D framework	V−F−V	this work
$[\{Cu_2(bisterpy)\}V_2F_2O_2\{HO_3PCH_2PO_3\}\{O_3PCH_2PO_3\}]$	1D	isolated V(IV)/V(V) square pyramids	$\{Cu_2V_2F_2O_2(O_3P\text{-})_3(HO_3P\text{-})\}$ chain	no	ref 42
$[\{Cu_2(bisterpy)\}V_2F_2O_2(H_2O)_2\{HO_3P(CH_2)_2PO_3\}]$	2D	isolated V(IV) square pyramids	$\{Cu_2V_2F_2O_2(O_3P\text{-})_2(HO_3P\text{-})_2\}$ cluster	no	ref 42
$[\{Cu_2(bisterpy)\}V_2F_4O_4\{HO_3P(CH_2)_2PO_3H\}]$	1D	isolated V(V) trigonal bipyramids	$\{CuVF_2O_2(HO_3P\text{-})]$ cluster	no	ref 42
$[\{Cu_2(bisterpy)\}_3V_8F_6O_{17}\{HO_3P(CH_2)_3PO_3\}_4]$	3D	isolated V(IV) square pyramids; binuclear units of corner-sharing V(V) tetrahedra; tetranuclear rings of edge-sharing V(V) square pyramids	$\{Cu_2V_2O_5(O_3P\text{-})_2\}$ chains, $\{V_4O_8F_4(HO_3P\text{-})_2\}^{2-}$ clusters	V−O−V	ref 42
$[\{Cu_2(bisterpy)(H_2O)_2\}V_2F_2O_2\{O_3P(CH_2)_3PO_3\}\{HO_3P(CH_2)_3PO_3\}]$	2D	isolated V(IV) square pyramids	$\{Cu_2V_2F_2O_2(O_3P\text{-})_3(HO_3P\text{-})\}$ clusters	no	ref 42
$[\{Cu_2(bisterpy)\}V_4O_6F_2\{O_3P(CH_2)_4PO_3\}_2]$	3D	isolated V(V) tetrahedra; binuclear units of corner-sharing V(IV) square pyramids	$\{CuV_2O_3F(O_3P\text{-})_2\}$ layers	V−F−V	ref 42
$[\{Cu_2(bisterpy)\}V_4F_4O_4(OH)(H_2O)\{HO_3P(CH_2)_5PO_3\}\{O_3P(CH_2)_5PO_3\}]$	2D	isolated V(IV) square pyramids; binuclear units of corner-sharing V(IV) square pyramids	$\{Cu_2V_4O_4F_4(OH)(H_2O)(O_3P\text{-})_3(HO_3P\text{-})\}$ clusters	V−O−V	ref 42
$[\{Cu_2(bisterpy)(H_2O)\}_2V_8O_8F_4(OH)_4\{HO_3P(CH_2)_5PO_3H\}_2\{O_3P(CH_2)_5PO_3\}_3]$	3D	binuclear units of corner-sharing V(IV) square pyramids	$\{Cu_4V_8O_8F_4(OH)_4(HO_3P\text{-})_4(O_3P\text{-})_6\}$ clusters	V−O−V	ref 42

building block, as noted in Table 7. In fact, even the common $\{M_2P_2O_4\}$ and $\{M_2PO_3\}$ secondary building units[68,69] are not universal structural motifs in the latter series of compounds. Consequently, one encounters a dramatic structural variability manifested in five unique structures as the organic spacer of the diphosphonate groups -$(CH_2)_n$- is varied from $n = 2-5$. Furthermore, there are no structural analogies between the copper-containing series of materials and those of this study.

The structural diversity associated with the oxyfluorovanadium materials is derived from a number of geometric determinants. Most obvious is the identity of the charge-compensating cation or secondary metal complex cation (SMCC). In contrasting the inorganic substructure of the two series of compounds, it is evident that the incorporation of the sterically demanding SMCC, $\{Cu_2(bisterpy)\}^{4+}$, disrupts the spatial expansion of the inorganic substructure Cu/V/P/O/F. Thus, the inorganic components of the oxyfluorovanadium/copper-bisterpy/diphosphonate family are generally small oligomeric units with only one instance each of one-dimensional (1D) and 2D substructures. In contrast, the inorganic substructures of the oxyfluorovanadium/diphosphonate family are 2D and 3D.

The tether length -$(CH_2)_n$- of the diphosphonate component also influences the overall polyhedral connectivity pattern. For $n = 3$, 4, and 5, the organic chains serve to buttress the inorganic layers and are consequently sandwiched between V/P/O/F networks in the common pillared layer structural motif. In contrast, for the two structures with $n = 2$, the organic spacers provide an integral component of $[V_6F_7O_6\{O_3P(CH)_2PO_3\}_4]_n^{4n-}$ and $[V_2F_2\{O_3P(CH_2)_2PO_3\}_2]_n^{4n-}$ layers with $\{VO_6\}$ octahedra providing the pillaring units. Apparently, longer tether lengths predispose spatial expansion through the bridging diphosphonate scaffolds, while the ethylenediphosphonate ligand is sufficiently small to be accommodated *within* the layer substructure.

It is noteworthy that reduction of the vanadium sites is common to both series of compounds. However, the oxyfluorovanadium/copper-bisterpy/diphosphonate series exhibits reduction to the V(IV) state, or mixed valence V(IV)/V(V) species, and one instance of a V(V) species. In contrast, reduction to V(III) is observed in three of the five structures of the oxyfluorovanadium/diphosphonates of this study. Because V(III) generally adopts more or less regular octahedral geometry (short {V═O} bonds are precluded) considerable structural diversity is introduced in the polyhedral connectivity of V(III) octahedra, V(IV) square pyramids or octahedra, and phosphorus tetrahedra. This versatility is most apparent in the catenation of V(III) octahedra to provide the 1D substructures of **3** and **5**. In contrast, the vanadium building blocks of the oxyfluorovanadium/copper-bisterpy/diphosphonate series are isolated polyhedra or small clusters.

(68) Férey, G. *J. Solid State Chem.* **2000**, *152*, 37.
(69) Férey, G. *Chem. Mater.* **2001**, *13*, 3084.

Several observations on the consequences of fluoride incorporation are relevant. The range of V/F ratios for **1**−**5** is 1.78−0.5, which is quite similar to the range previously observed for other oxyfluorovanadium phosphates and phosphonates (2.5−0.5). However, such structures have exhibited O(OH)/F ratios in the range 1:1−4:1 with a concentration at 1:1. While **2** and **4** show ratios of 1:1 and 1.5:1, respectively, compound **1** is relatively oxo-group deficient at O/F of 0.5:1. Furthermore, there are two instances of exclusively reduced V(III) sites in the structures (**3** and **5**) and consequently an absence of terminal {V═O} linkages. Considerable variation in fluoride incorporation can be tolerated in these materials and considerable variation in the V−F bond distances, 1.75−2.19 Å, is possible. In addition, the fluoride may act as a terminal ligand or as a bridging group.

As previously noted, the range of architectures and substructural building blocks displayed by these materials also reflects the variations in P−O or P−OH bond distances and the "softness" of the M−O−P angle.[70] The incorporation of the $\{O_3PR\}$ tetrahedra as fully deprotonated, monoprotonated, or even diprotonated residues, which function as noncoordinating pendants or mono-, bi-, or tridentate donor groups, further expands the structural possibilities. Furthermore, the phosphorus tetrahedra may engage in corner- or edge-sharing interactions.

An additional structural variable is the possibility of incorporation of coordinated aqua ligands. It is curious that all the structures of this study (**1**−**5**) exhibit $V-OH_2$ bonding, while only 2 of 8 structures of the oxyfluorovanadium/copper-bisterpy/diphosphonate series contain aqua ligands to vanadium. Aqua ligation is common for V(III) species in general, which reflects the coordination preferences of this oxidation state.

A final point relates to the framework density of these materials. Structures **1**−**3** exhibit 13.5, 10.2, and 10.2 M atoms (M = V, P)/1000 $Å^3$, compared to 11.1 and 13.2 M atoms/1000 Å for **4** and **5**, respectively, which encapsulate large amounts of water of crystallization (7.1 and 12 wt %, respectively). It is evident that the accessible void volume in this series of compounds does not correlate with the framework density but rather reflects the detailed polyhedral connectivity that is adopted by the material.

Thermal Analyses. The thermal behavior of the open-framework compounds **4**·$7H_2O$ and **5**·$3.5H_2O$ was investigated. As illustrated in Figure 6, the TGA profile of **4**·$7H_2O$ exhibits a weight loss of ca. 8.0% in the 50−250 °C range, which is associated with the loss of water crystallization (7.8% theoretical weight loss for seven water molecules). This initial dehydration step is followed by a gradual weight loss of ca. 2% between 250 and 400 °C, and a final weight loss of 9% between 400 and 600 °C. The subsequent weight losses correspond to the loss of the ethylenediammonium cations and of the hydrocarbon component of the organophosphonate ligands with contaminant oxidation of the

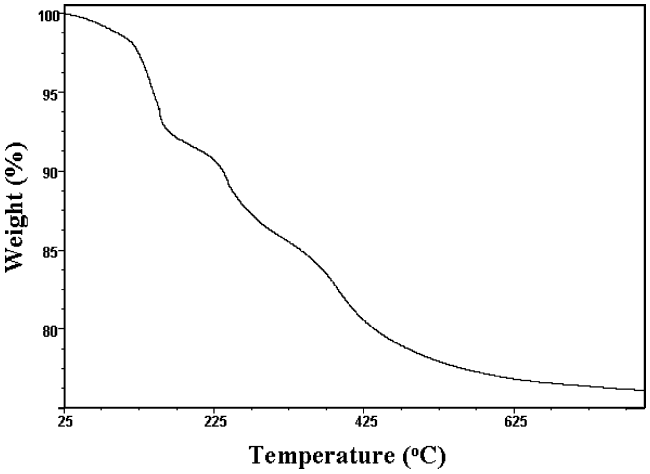

Figure 6. Thermogravimetric profile for **4** in the temperature range of 30−800 °C.

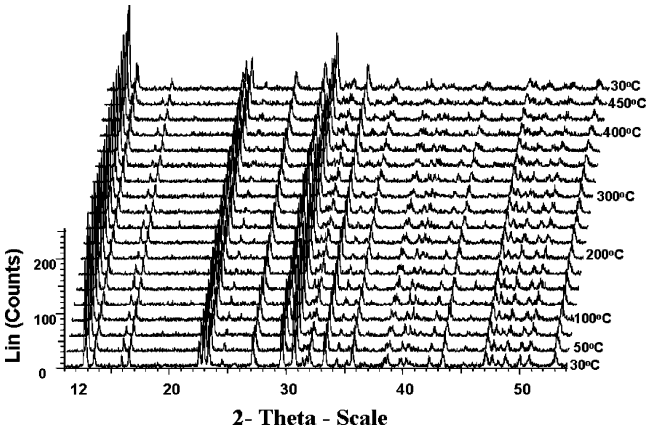

Figure 7. Thermodiffraction pattern of **4** in the temperature range of 30−450 °C.

phosphorus sites (theory: 10.5%). The thermodiffraction pattern for compound **4** in the 25−450 °C temperature range is shown in Figure 7. The profile shows that dehydration results in a phase isostructural with the parent compound. The diffraction profile is largely unchanged to 450 °C, which indicates that the oxyfluorovanadium/diphosphonate framework is thermally robust and persistent to ca. 450 °C. Above 450 °C, decomposition of the organophosphonate ligand results in an amorphous phase that was not characterized.

The infrared spectra of samples of **4** at room temperature, 175 °C, 350 °C, and 650 °C, shown in Figure 8, are consistent with these observations.[71−73] The spectra show loss of the H_2O stretch and bend vibrations at 3540 and 1641 cm^{-1}, respectively, by 350 °C. Curiously, the organoammonium NH stretching and CH_2 bending modes at 2900−3350 and 1442 cm^{-1}, respectively, are not totally absent at 350 °C, which suggests that the ammonium cation decomposition occurs over a broad temperature range. This is confirmed by elemental analysis of a sample of **4** heated at 350 °C to constant weight, which is consistent with the presence of

(70) Huminichi, D. M. C.; Hawthorne, F. C. *Rev. Mineral. Geochem.* **2002**, *48*, 123.

(71) Bellamy, L. J. *The Infrared Spectra of Complex Molecules;* Wiley: New York, 1975.
(72) Hayashi, S.; Unemura, J. *J. Chem. Phys.* **1976**, *63*, 1732.
(73) Socrates, G. *Infrared Characteristic Group Frequencies;* Wiley: Chichester, England, 1980.

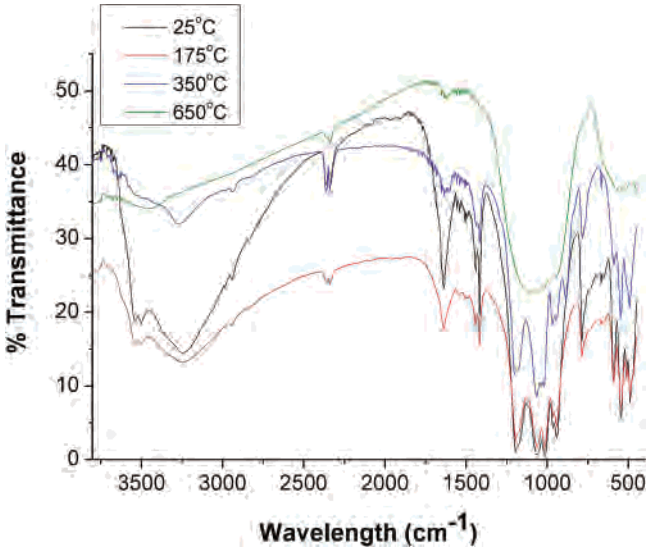

Figure 8. Infrared spectra of **4** at room temperature (black), 175 °C (red), 350 °C (blue), and 650 °C (green) in the range of 500−4000 cm^{-1}.

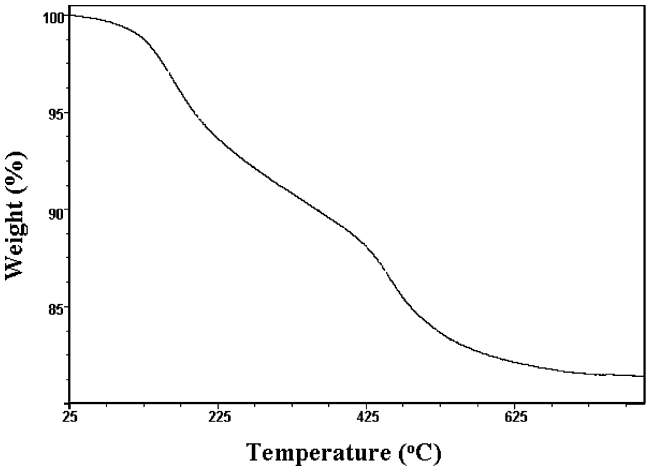

Figure 9. TGA curve for **5**.

one ammonium cation for each oxyfluorovanadium−organodiphosphonate formula unit. The elemental analysis of this dehydration product is consistent with the mixed valence formulation $[NH_4][V_7O_7F_4\{O_3P(CH_2)_2PO_3\}_4]$, indicative of the essential retention of the structure of the anionic framework.

The infrared spectrum in the 780−1200 cm^{-1} region in which the V−O and P−O stretching modes are found largely retains its characteristic features at 350 °C, which again is consistent with the structural integrity of the framework of **4** at these temperatures.

The TGA profile of **5**·$3.5H_2O$, shown in Figure 9, is characterized by a weight loss of ca. 23.9% in three steps between 50 and 600 °C. The initial weight loss of 8.5% in the 50−180 °C range corresponds to the loss of 3.5 water molecules of crystallization (9.3%, theoretical weight loss). The loss of 5.8 wt % in a second step between 200 and 325 °C is consistent with a second dehydration step (5.3%, theoretical weight loss for two water molecules). A final weight loss of 9.5% is consistent with decomposition and oxidation of the phosphorus sites. The product of the thermal decomposition is amorphous and was not further characterized. The thermodiffraction profile of **5** (Figure 10) is considerably more complex than that of **4**. There is minimal structural change through the initial dehydration (30−180 °C), which indicates that the framework structure is maintained without collapse in the partially dehydrated material. However, above 200 °C a new phase appears that persists to ca. 450 °C. This observation is consistent with previous studies that indicate that the frameworks exhibit structural rearrangement concomitant to the loss of coordinated water molecules. However, the framework does not collapse and that crystallinity is retained to ca. 450 °C.

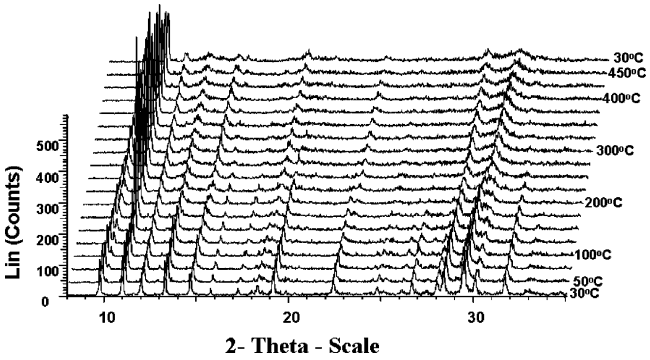

Figure 10. Thermodiffraction patterns for **5** in the temperature range of 30−425 °C.

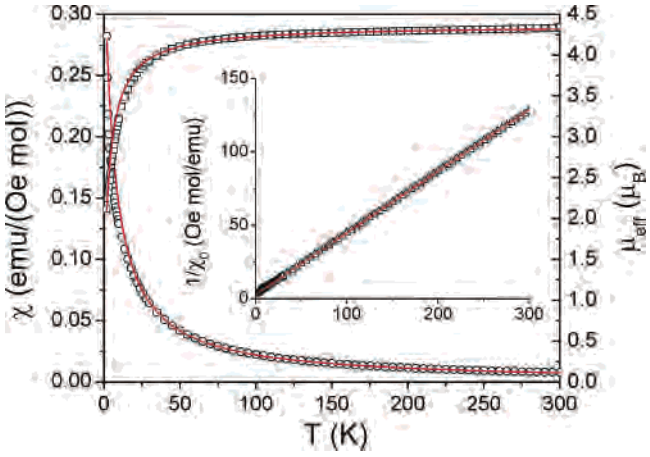

Figure 11. The dependence of the magnetic susceptibility χ (○), the effective magnetic moment μ_{eff} (□) and the reverse susceptibility χ_o (△) of **1** on temperature. The lines drawn through the data points are the fits to the Curie−Weiss law.

Magnetic Properties. Organic−inorganic hybrid materials provide new opportunities in the realm of molecular magnetism for studying magnetically condensed systems, that is, exchange-coupled materials. In such compounds, low-dimensional arrangements of the magnetic ions are achieved through the use of nonmagnetic dividers such as phosphate donor groups and the organic substituents. In the compounds of this study, different orientations of the paramagnetic V(III) and/or V(IV) sites result in quite unique descriptions of the magnetism.

The paramagnetism of compound **1** arises from both V(IV) and V(III) sites, d^1 and d^2, respectively. The temperature variation of the magnetic susceptibility was fit to the Curie−Weiss law (eq 1) (Figure 11). The best fit gave $C = 2.38$ emu K/(Oe mol), $\Theta = -6.6$ K, $\chi_{TI} = -0.00028$ emu/(Oe

mol). The effective moment at 300 K is μ_{eff} (300 K) = 4.33 μ_B, which corresponds to two $S = 1/2$ ions and two $S = 1$ ions, with $g = 2.06$.

$$\chi = \chi_o + \chi_{TI} = \frac{C}{T - \Theta} + \chi_{TI} \quad (1)$$

Compounds **3**−**5** similarly exhibit Curie−Weiss law dependence of the magnetic susceptibilities at high temperatures. For compound **3**, the best fit provided $C = 3.95$ emu K/(Oe mol), $\Theta = -19.2$ K, $\chi_{TI} = 0.0016$ emu/(Oe mol). The effective magnetic moment $\mu_{eff} = \sqrt{8\chi_o T}$ at 300 K is 5.45 μ_B, which corresponds to six V(III) ions with $S = 1$, $g = 1.85$.

The fit for compound **4**·7H_2O yields $C = 2.68$ emu K/(Oe mol), $\Theta = -3.4$ K, $\chi_{TI} = -0.00051$ emu/(Oe mol). The effective magnetic moment at 300 K is μ_{eff} (300 K) = 4.60 μ_B, corresponding to seven V(IV) ions with $S = 1/2$, $g = 2.02$. In the case of compound **5**·3.5H_2O, the best fit gave $C = 2.12$ emu K(Oe mol), $\Theta = 1.7$ K, $\chi_{TI} = 0.00053$ emu/(Oe mol). The effective magnetic moment at 300 K is 4.13 μ_B, which is consistent with two V(III) ions with $S = 1$, $g = 2.06$. The increase in the effective moment with decreasing temperature to 14 K arises from chain ferromagnetic exchange interactions. The decrease in the effective moment with decreasing temperature below 14 K indicates the existence of a secondary antiferromagnetic chain exchange interaction.

The temperature dependence of the magnetic susceptibility of **2** is plotted in Figure 12. The maximum at 9.5 K indicates the presence of antiferromagnetic interactions. The best description of the experimental results has been obtained using the Heisenberg linear antiferromagnetic chain model for V(IV) with $S = 1/2$ taking into account the presence of monomeric paramagnetic impurities with concentration p (equation 2).[76]

$$\chi = \frac{2N_A g^2 \mu_B^2}{k_B T} \frac{0.25 + 0.14995y + 0.30094y^2}{1 + 1.9862y + 0.66854y^2 + 6.062y^3} + \chi_{TI} \quad (2)$$

$$y = |J|/k_B T$$

The best fit gave $g = 1.85$ $J/k_B = -7.32$ K, $\chi_{TI} = -0.00054$ emu/(Oe mol), $p = 0.001$. The effective magnetic moment at 300 K is 2.35 μ_B, which is consistent with two V(IV) sites.

While the V/P/O/F substructure of **2** is 2D, the magnetic behavior conforms to a 1D model. Such descent in dimensionality of the magnetic exchange mechanism is not unusual in solids. In general, oxovanadium(IV) phosphates exhibit magnetic behaviors that cannot be deduced exclusively from their overall structural features. This is because of the involvement of phosphate bridges in the spin transfer between V(IV) centers.[77] For example, the 2D materials $(NH_4)VOPO_4$[78] and β-$VO(HPO_4)$·2H_2O[79] and the 3D phase $VO(H_2PO_4)_2$[79] exhibit magnetic properties consistent with the Heisenberg antiferromagnetic chain model.[80]

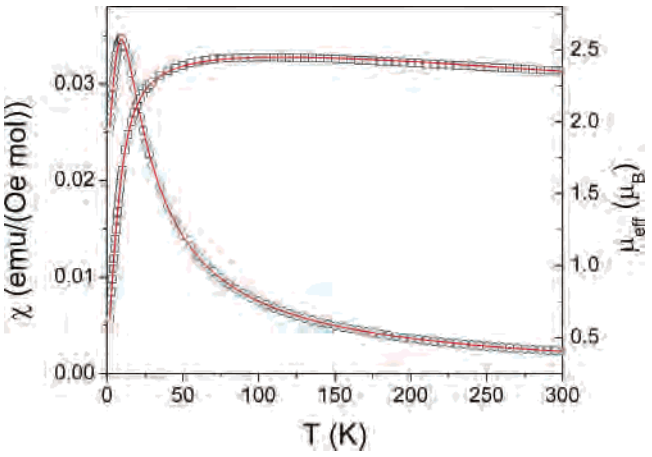

Figure 12. The dependence of the magnetic susceptibility χ (○) and of the effective magnetic moment μ_{eff} (□) of **2** on temperature. The lines drawn through the data are the fits to the Heisenberg linear antiferromagnetic chain model.

Conclusions. Hydrothermal reaction conditions provide a convenient method for the synthesis of organic/inorganic hybrid materials of the oxyfluorovanadium/organodiphosphonate family. Variations in reaction conditions and the spacer length of the diphosphonate ligand in the presence of fluoride provided the pillared layer phase **1**, the 2D phases **2** and **3**, and the 3D materials **4**·7H_2O and **5**·3.5H_2O. The pillared layer structural motif, which was previously described as a recurrent theme of the oxovanadium/organodiphosphonate and oxovanadium/organodiphosphonate/organoammonium families of materials,[44] is represented in the overall 3D structure of **1** and in the pillared double layer structures of **2** and **3**. However, materials **4** and **5** exhibited complex 3D inorganic substructures for their V/P/O/F frameworks. In contrast to the fluoride materials of the oxyfluorovanadium/copper-bisterpy/organodiphosphonate family, which exhibit isolated vanadium polyhedra and binuclear units as structural subunits, a variety of vanadium building blocks are embedded in the structures of **1**−**5** including isolated octahedra, binuclear units, trinuclear clusters, and chains. Furthermore, compound **4** manifests both binuclear and trinuclear motifs, while **5** contains isolated octahedra and chains of edge-sharing octahedra.

At the higher fluoride concentrations necessary for the incorporation of fluoride into the inorganic substructures of these materials, reduction to the V(III) oxidation state occurred in three instances. While such reduction was

(74) Riou-Cavellac, M.; Serre, C.; Férey, G. *C. R. Acad. Sci., Ser IIc: Chim.* **1999**, *2*, 147.
(75) Bonavia, G.; Haushalter, R. C.; Zubieta, J. *J. Solid State Chem.* **1996**, *126*, 292.
(76) Estes, W. E.; Gavel, D. P.; Hatfield, W. E.; Hodgson, D. J. *Inorg. Chem.* **1978**, *17*, 1418.
(77) Amoros, P.; Beltran, A.; Beltran, D. *J. Alloys Compd.* **1992**, *188*, 123.
(78) Haushalter, R. C.; Chen, Q.; Soghomonian, V.; Zubieta, J.; O'Connor, C. J. *J. Solid State Chem.* **1994**, *108*, 128.
(79) Beltran-Porter, D.; Beltran-Porter, A.; Amoros, P.; Ibanez, R.; Martinez, G.; LeBail, A.; Ferey, G.; Villeneuve, G. *Eur. J. Solid State Inorg.Chem.* **1991**, *28*, 131.
(80) Villeneuve, G.; Amoros, P.; Beltran, D.; Drillen, M. In *Organic and Inorganic Low Dimensional Crystalline Materials*; Delkaes, P., Drillen, M., Eds., NATO Asi Series; Plenum Press: New York, 1987; Vol. B168, p 417.

previously reported for phosphate phases of vanadium,[74,75] incorporation of V(III) sites was not observed for the materials of the oxyfluorovanadium/copper-bisterpy/organodiphosphonate family.

A number of structural determinants may be significant including the polyhedral and oxidation state variability of vanadium, the promiscuous possibilities for vanadium and phosphorus polyhedral connectivities, flexibility of P−O(H) bond distances and V−O−P bond angles, variable protonation of $\{PO_3\}$ groups and vanadium oxo-sites, coordination of aqua ligands, incorporation of varying ratios of F−V, and the organic tether lengths. The more complex 3D structures **4** and **5** are obtained with the shortest tether length of this study, $n = 2$. It appears that longer spacers tend to provide spatial extension by buttressing anionic inorganic networks, while the shorter ethylenediphosphonate ligand can be accommodated within a layer substructure, resulting in more complex connectivities. The absence of a structural systematic for these materials reflects this diversity of structural determinants and the dynamic synergism between the component building blocks in the hydrothermal domain.

The oxyfluorovanadium/diphosphonate frameworks of these materials are thermally robust and may be retained well past the dehydration temperature. The sorptive properties of the dehydrated material **4′**, as well as synthetic approaches to other vanadium−phosphonate phases incorporating fluoride, are under investigation.

Acknowledgment. This work was funded by a grant from the National Science Foundation, CHE-0604527.

Supporting Information Available: Crystallographic files in CIF format for compounds **1**−**5**. Supplementary Figures 1−3, showing the dependences of the magnetic susceptibility, the effective magnetic moment, and the reverse susceptibility of **3**−**5** on temperature. This material is available free of charge via the Internet at http://pubs.acs.org.

IC0604462